The Report Committee for Yalin Yu
Certifies that this is the approved version of the following report:

Measurement of adhesion between soft elastomers with different mixing ratios

APPROVED BY
SUPERVISING COMMITTEE:

Supervisor:

Nanshu Lu

Chad M. Landis

Measurement of adhesion between soft elastomers with different mixing ratios

by

Yalin Yu, B.E.; M.E.

Report

Presented to the Faculty of the Graduate School of

The University of Texas at Austin

in Partial Fulfillment

of the Requirements

for the Degree of

Master of Science in Engineering

The University of Texas at Austin

May 2014

Dedication

To my mother and brothers. Without their great love, I can never complete this work.

Acknowledgements

First of all, I would like to express my deep gratitude to my advisor Dr. Nanshu Lu for teaching and guiding me with patience and dedication during the past two years. Without her helpful guidance and constant support, this work could not be possible. I am also grateful to Dr. Kenneth M. Liechti for his enlightening discussions and ideas to overcome various difficulties in experiments.

I would like to thank Dr. Chad M. Landis for being one of the readers of this report. His careful review and insightful suggestions make the report much better than it was.

I would also like to thank all of the members in Dr. Lu's group. Emil and Soo helped me build the initial JKR apparatus and got preliminary experimental data and later Soo and Becky spent a semester on making a humidity chamber for the future study on the effect of humidity. Also, Becky and Danny did a great favor in my experiments. Being undergraduates students, they are young but they did excellent work in the lab. Without them, my research progress would be much slower and my life would not be so exciting.

Finally, I would like to thank the National Science Foundation for the financial support.

Abstract

Measurement of adhesion between soft elastomers with different mixing ratios

Yalin Yu, M.S.E.

The University of Texas at Austin, 2014

Supervisor: Nanshu Lu

The JKR method is widely used to measure the work of adhesion between soft materials. In this report, the JKR theory is summarized and three dimensionless parameters are proposed as prerequisites to determine sample dimensions in designing experiments. Also, the work of adhesion between two commonly used soft elastomers PDMS (Sylgard 184) and Ecoflex 0300 are obtained with the measured pull-in and pull-off forces from a dynamical mechanical analyzer. The Young's moduli of pristine PDMS are also calculated with a two point formula and the results are compared with that from tensile tests.

Our results for the work of adhesion of pristine PDMS 10:1 agree well with those reported in the literature. The pull-off work of adhesion of pristine PDMS increases significantly as the mixing ratio increases from 10:1 to 20:1. With further increasing mixing ratios, the pull-off work of adhesion does not change much. However, for PDMS samples extracted with chloroform, the pull-off work of adhesion increases monotonically as the mixing ratio varies from 10:1 to 50:1. A similar trend is also

observed for the case of contacts between pristine PDMS lenses and Ecoflex substrates. For the pull-in work of adhesion, the results are almost independent of the mixing ratios.

An adhesion mechanism is proposed to explain these complex adhesion behaviors. It is concluded that the entanglement with each other and penetration into networks of tethered chains during the contact could enhance the pull-off work of adhesion. With both ends uncross-linked, free chains do not enhance the pull-off work of adhesion as significant as tethered chains. Therefore, for pristine PDMS with higher mixing ratios, the existence of more free chains reduces the chance of the entanglement and penetration of tethered chains, which compensates for the enhancement by more tethered chains.

Table of Contents

List of Tables

List of Figures

Chapter 1: Introduction

1.1 BACKGROUND

The phenomenon of adhesion is ubiquitous both in nature and in our daily life. Animals like insects, spiders and lizards use their biological attachment pads to provide the support and mobility to their bodies. These adhesive attachment pads often consists of a very flexible superficial layer covered by fine patterns of protuberances of different origins (see Figure 1) [1, 2]. Using these adhesive pads on their limbs, animals can attach themselves on various different surfaces.

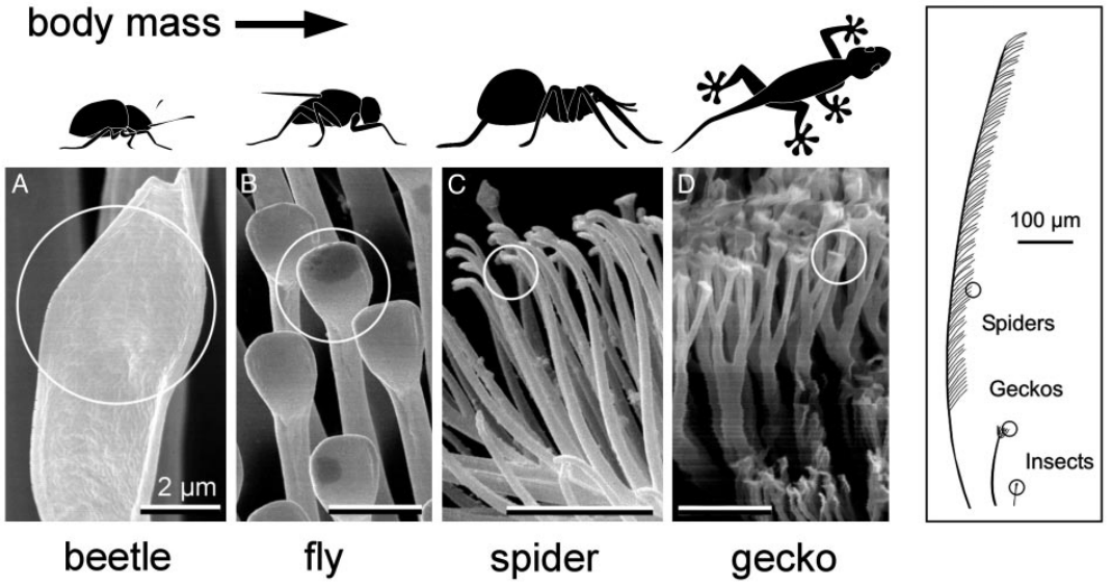

Figure 1: Animals and their hairy attachment pads [1].

Adhesion is also widely used in engineering and technology applications. Recently, great progress has been made in bio-integrated electronics [3-6]. However, to further improve the performance of bio-integrated electronics, one of the essential challenges is to achieve intimate contact at the interfaces between electronics and soft

tissues. Therefore, it is necessary to measure and understand the adhesion at these interfaces.

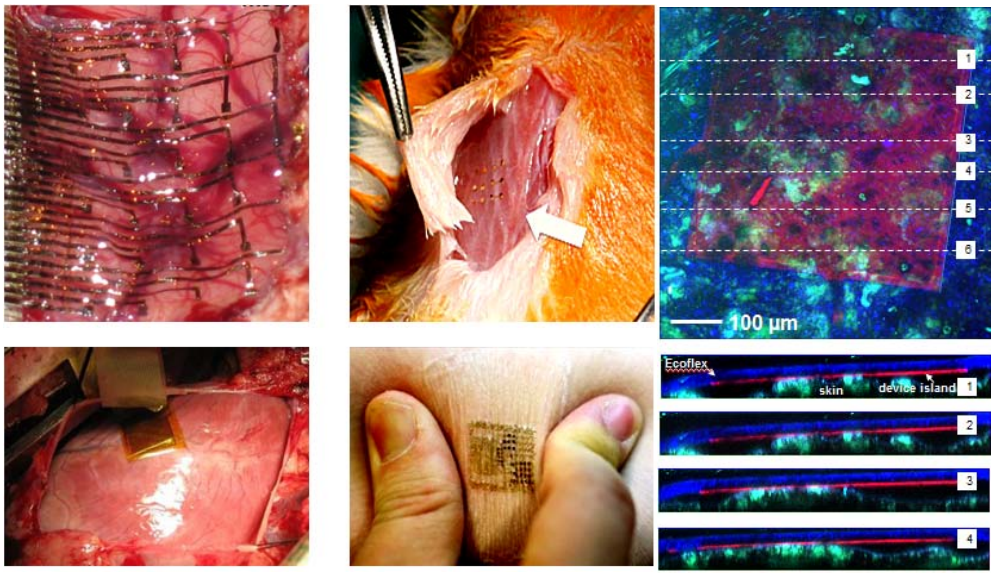

Figure 2: Various bio-integrated electronics and their interfaces [3-6].

In making bio-integrated electronics, electronic devices were usually grown or deposited on silicon wafers and would be transferred to an elastomer substrate later with a stamp, like PDMS. To make sure that the transfer-printing succeeds, first, the adhesion between the device and stamp should be stronger than that between the device and the silicon wafer so that the device can be pulled off from the wafer. Also, the adhesion between the device and the target elastomer substrate should be stronger than that between the device and the stamp so that the device can stay on the target elastomer substrate.

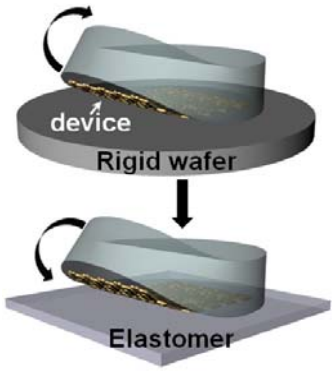

Figure 3: Transfer-printing process.

1.2 OBJECTIVE

The objective of this report is to develop a systematic and sound experimental method to measure the work of adhesion between soft elastomers and to use this method to explore the basic mechanisms of adhesion between soft elastomers.

Once the experimental method is validated, it can be generalized to study the work of adhesion between other materials, like biological tissues and elastomers, or tissue and gold. Knowing the work of adhesion between materials, it is also useful to be able to predict the conformability and crack propagation at interfaces with theoretical and numerical analyses. Such results will provide further guidance in the design of structures and bio-electronics to improve their performances.

As mentioned, another important goal is to explore the basic mechanisms of adhesion between soft elastomers. Understanding those basic mechanisms will enable us to tune the adhesion for different applications.

To achieve these goals, first, the important results from the JKR theory are summarized and the applicable conditions are discussed. Then, a detailed review of the existing experimental work is given and based on that, careful experiments were design

and conducted on soft elastomers. Finally, experimental results are compared and discussed followed by the conclusions and the recommendations for the future work.

1.3 JKR THEORY

In the field of contact mechanics, there are many different theoretical models to describe the deformation of solid materials that are placed in contact with one another. These models are based on various assumptions and therefore apply under different situations.

The pioneering and fundamental work in contact mechanics was contributed by Hertz in 1882 when he was studying Newton's optical interference fringes between two glass lenses. In Hertz's contact model, the stresses within the contacted area are purely induced by the elastic deformation and the adhesive forces between materials are not taken into account. Therefore, the Hertz contact model is essentially non-adhesive.

When an elastic sphere contacts with an infinite elastic half space, the following two contact equations describe the relations between the applied load P, the penetration δ and the contact radius a for Hertz's theory [7, 8].

$$a^3 = \frac{3PR}{4E^*} \tag{1}$$

$$\delta = \frac{a^2}{2R} \tag{2}$$

where R is the radius of the sphere and E^* is the combined elastic modulus of the two materials and it is defined by

$$\frac{1}{E^*} = \frac{1-\nu_1^2}{E_1} + \frac{1-\nu_2^2}{E_2} \tag{3}$$

where E_1, E_2, ν_1 and ν_2 are the Young's moduli and Poisson's ratios of the two bodies in contact, respectively. If two different spheres contact with each other, the radius R should be replaced by

$$\frac{1}{R} = \frac{1}{R_1} + \frac{1}{R_2} \tag{4}$$

where R_1 and R_2 are the radii of the two spheres in contact.

The assumptions that Hertz adopted in the derivations of the equations above are summarized below:

(i) both the materials are homogenous and isotropic

(ii) the strains are small and within the scope of the linear elastic theory

(iii) the surfaces are continuous, non-conforming and frictionless

(iv) each body is regarded as an infinite elastic half space during the contact and the contact radius is much smaller than the characteristic curvature radius of the bodies

(v) adhesion between the two bodies can be neglected.

Since Hertz's theory is based on linear elasticity, we have the assumption (ii). Furthermore, both the frictional and adhesive forces are not considered in the derivations, which is the origin of the assumptions (iii) and (v). Assumption (iv) allows for the use of the solutions for the distributed load on an elastic half space.

Hertz's theory works well when the effects of adhesion can be neglected, as in the case where the applied load is quite large compared to the adhesive force between the two bodies in contact. However, when the surfaces in contact are smooth, clean and dry, the adhesion can be very strong and therefore cannot be neglected, especially when the applied load is comparable to the adhesive force. Many experiments show that at high loads, the results fit the Hertz theory closely, while at low loads the contact areas between the two bodies were considerably larger than those predicted by Hertz theory [9]. For examples, when the applied load was reduced to zero, the contact area did not vanish as predicted by the Hertz theory, but tended towards a constant value. Also, to separate two

bodies in intimate contact, a tensile loading must be applied to overcome the adhesive forces. To explain these experimental phenomena and to better predict the behavior between adhesive solids, adhesion should be taken into account between the two bodies in contact.

For two rigid spheres, Bradley showed in 1932 that the pull-off force P_{po} to separate them was given by [10]

$$P_{po} = -2\pi WR \tag{5}$$

where R is given by equation (4) and W is the work of adhesion. For deformable spheres, in 1971 Johnson et al. proposed an adhesive model which is now called the JKR theory [9]. They also performed experiments on the contact of rubber and gelatin spheres to support their theory. However, in 1975 Derjaguin et al. proposed a different adhesive model which is called the DMT theory [11]. These two theories were contradictory in some aspects such that it raised a hot debate at that time. One of the obvious differences between the two theories is the prediction of the pull-off force. The DMT theory retains the equation (5) while for the JKR theory, the coefficient is 1.5 instead of 2. Fortunately, this situation was resolved just two years later by Tabor who suggested that these two models were both valid under different circumstances corresponding to the opposite extremes of the Tabor parameter, μ, which represents the ratio of the elastic displacement of the surfaces at the point of pull-off to the effective range of surface forces [12, 13]. The JKR theory applies to large, compliant spheres for large μ while the DMT theory applies to small, stiff spheres for small μ. Using a Dugdale model, Maugis proposed the MD theory that could describe the continuous transition between DMT and JKR theories as the Tabor parameter varied [14]. Based on this MD model, Johnson and Greenwood have constructed an "adhesion map" with the Tabor parameter μ as the horizontal coordinate and the dimensionless applied load $\overline{P} = P/(\pi WR)$ as the

vertical coordinate (see Figure 4 below) [13, 15]. From the adhesion map, we can see that the Hertz model is on the top and therefore applies for large loads. At the bottom, the loads are light and the JKR theory applies for large μ. Using this adhesion map, we can decide which model is appropriate for different situations. Since the materials tested in our experiments are soft elastomers (PDMS or Ecoflex), the JKR theory will apply.

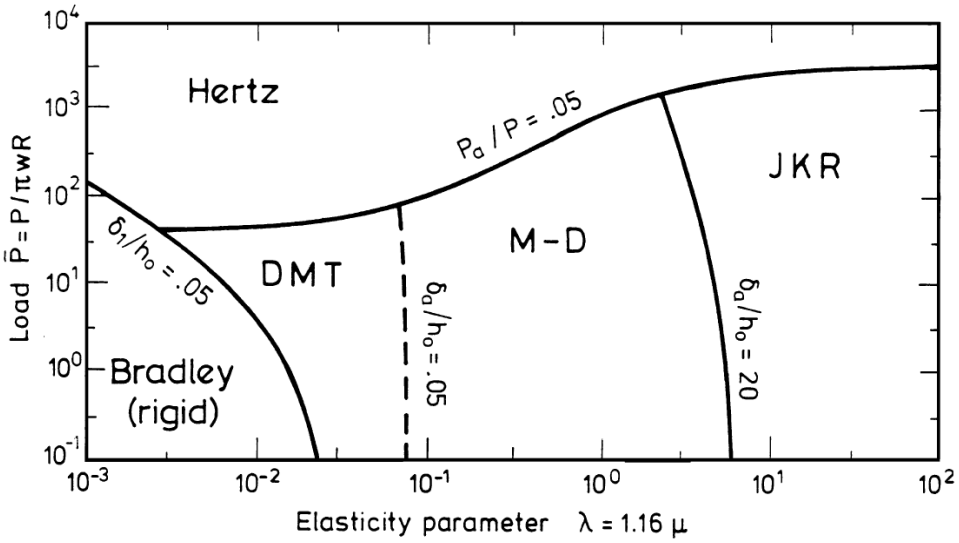

Figure 4: Adhesion map [13, 15].

To account for the effect of the work of adhesion, the contact equations for the JKR theory are given by [9, 16]

$$a^3 = \frac{3R}{4E^*}\left[P + 3\pi WR + \sqrt{6\pi WRP + (3\pi WR)^2}\right] \tag{6}$$

$$\delta = \frac{a^2}{3R} + \frac{P}{2E^* a} \tag{7}$$

When the work of adhesion is zero, i.e., $W = 0$, it recovers the case of the non-adhesive Hertz theory and therefore equations (6) and (7) are the same as equations (1) and (2). The load penetration curves for the Hertz and JKR theory are plotted below with dimensionless quantities.

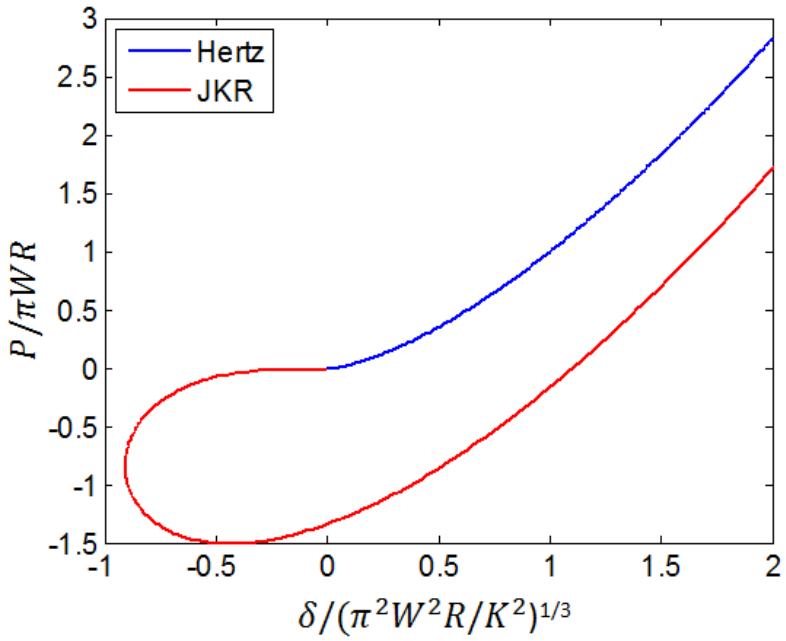

Figure 5: Dimensionless load vs. penetration curves for the Hertz and JKR theories.

When the work of adhesion is not zero, under the same load P, equation (6) shows that the JKR contact radius is larger than that in the Hertz theory.

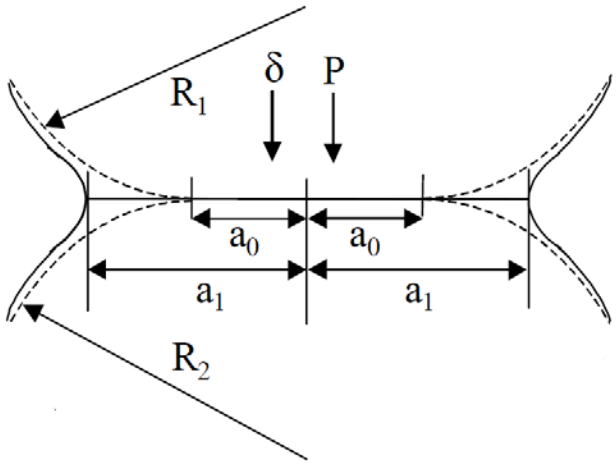

Figure 6: The contact between two elastic bodies in the presence (contact radius a_1) and absence (contact radius a_0) of adhesion [9]

In order for the contact radius to take on real values, the expressions under the square root in equation (6) should not be less than zero and the critical value of the load gives the pull-off force to separate the two bodies.

$$P_{po} = -\frac{3}{2}\pi WR \tag{8}$$

Notice that the pull-off force P_{po} is proportional to the work of adhesion W. What's more, the pull-off force is independent of the elastic properties.

When the contact occurs with an almost zero penetration, $\delta = 0$, the force becomes negative due to their attractive interaction. From equations (6) and (7), the pull-in force P_{pi} can be obtained as

$$P_{pi} = -\frac{4}{3}\pi WR\,. \tag{9}$$

Based on the JKR theory, a two-point formula was proposed to calculate the combined elastic modulus of the two bodies with data from nanoindentation [17-20]

$$E^* = \frac{-3P_{po}}{\sqrt{R}}\left[\frac{3\left(\delta_0 - \delta_{po}\right)}{1+4^{-2/3}}\right]^{-3/2} \tag{10}$$

where δ_0 is the corresponding penetration when the applied load is zero and δ_{po} is the penetration when the pull-off occurs. Since it involves information at only two points, it is often called a two-point formula. Notice that in the formula the combined modulus is related to the difference between the two penetration depths. Therefore, it is independent of the determination of the zero penetration.

For the JKR model of adhesion between two homogenous elastic solids, the adhesive forces outside the contact area are neglected. Therefore, this model only gives a good approximation when the adhesive forces are short range in comparison to the elastic deformation. That is, the non-dimensional Tabor parameter satisfies the following requirements:

$$\mu = \left(\frac{RW^2}{E^{*2} z_0^3} \right)^{1/3} > 5 \tag{11}$$

where R is the radius of curvature of the sphere, W is the work of adhesion, E^* is the combined Young's modulus, and z_0 is the equilibrium spacing between the contacting surfaces ($\approx 0.3nm$) [21, 22].

In practical experimental setups, the substrate with a finite thickness has to be placed on some solid stage while in the derivation of the JKR theory, the substrate is regarded as an infinite elastic domain. To eliminate the effect of the solid stage and keep consistency between the experiments and theory, the thickness is supposed to large enough to mimic an elastic half-space. Numerical results from the finite element method based on the JKR theory have shown that the pull-off force formula is valid when the dimensionless adhesion parameter α satisfies the following inequality [21, 22]

$$\alpha = \left(\frac{2WR^2}{\overline{E}_1 h^3} \right)^{1/2} < 0.02 \tag{12}$$

where $\overline{E}_1$ is the plane strain Young's modulus and h is the thickness of the substrate.

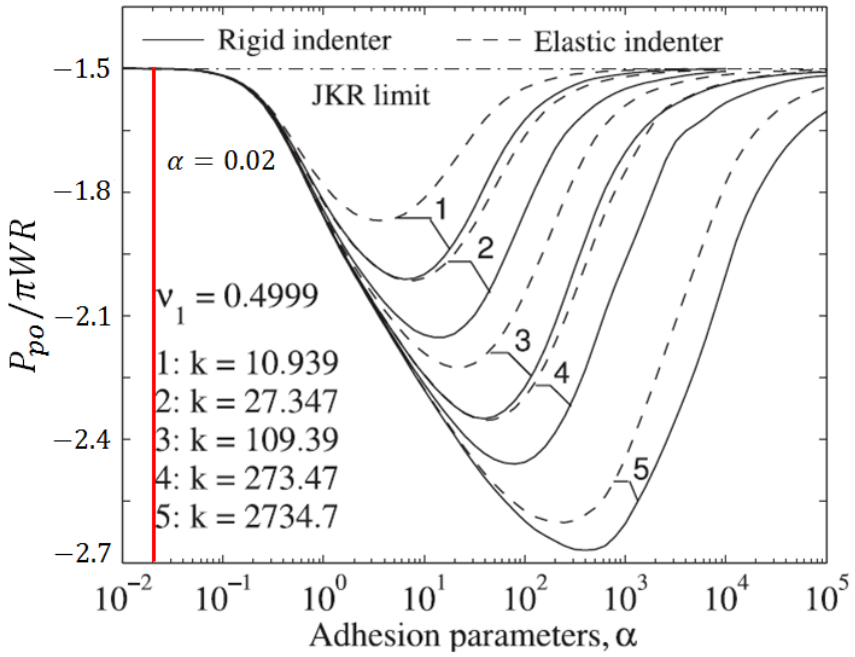

Figure 7: Normalized pull-off force vs. the adhesion parameter α [22].

In the derivation of the JKR equations, the parabolic approximation of the spherical profile is used for small contact radii in contrast to the actual radius of curvature of the sphere. For materials with low work of adhesion (44 mJ/m^2) and the curvature radius from 1-2 mm, this might be the case. However, for materials with a high work of adhesion, 500 mJ/m^2 and the same radius of curvature, even at the pull-off, the contact radius may be comparable to the curvature radius. Theoretical analysis using the exact spherical profile demonstrates that the pull-off force formula is approximately valid as long as the dimensionless parameter m is larger than 5 [23].

$$m = \left(\frac{RK}{\pi W} \right)^{1/3} > 5 \tag{13}$$

where $K = 4E^* / 3$. When m is small, the exact spherical profile should be used and the contact equations become

$$\Delta = \frac{mA}{2}\ln\frac{m+A}{m-A} - \frac{2}{3}\sqrt{6A} \tag{14}$$

$$\overline{P} = \frac{3m}{8}\left(m^2 + A^2\right)\ln\frac{m+A}{m-A} - \frac{3}{4}m^2 A - A\sqrt{6A} \tag{15}$$

where $\Delta = \dfrac{\delta}{\left(\pi^2 W^2 R / K^2\right)^{1/3}}$, $A = \dfrac{a}{\left(\pi W R^2 / K\right)^{1/3}}$ and $\overline{P} = \dfrac{P}{\pi W R}$ are dimensionless penetration, contact radius and load [23]. Using equation (15), one can determine the pull-off force for a given value of m. When $m = 5$, $P_{po} = -1.47\pi WR$ and the error induced by using the equation (8) is about 2%. Therefore, when $m > 5$, the induced error will be less than 2%.

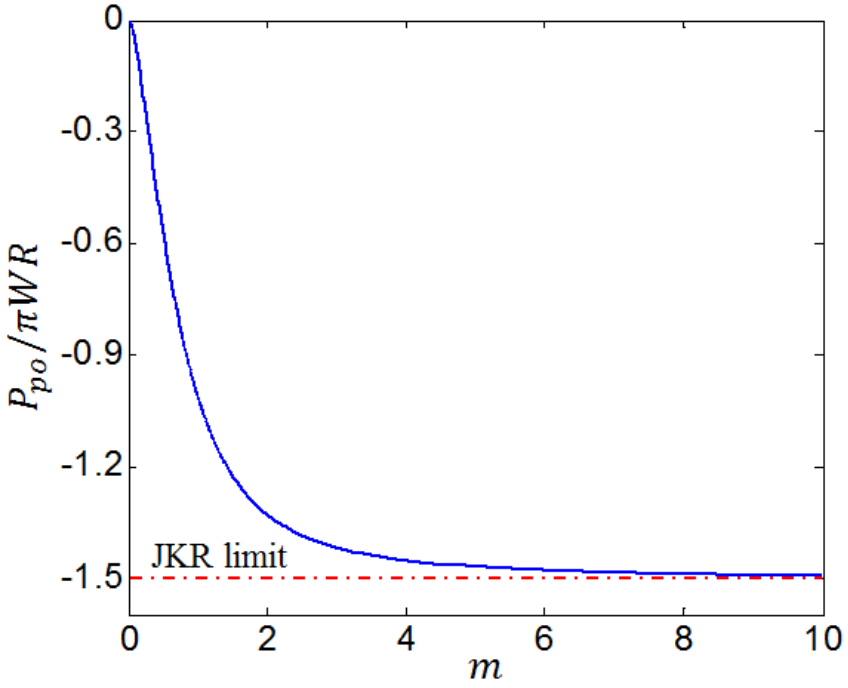

Figure 8: Normalized pull-off force vs. m [23].

1.4 EXISTING WORK

Using the JKR theory, the work of adhesion between two solid materials can be measured directly from the contact experiments.

In their paper outlining the JKR theory, Johnson et al. conducted contact experiments between two rubber spheres of radius 2.2 cm in air, water and a 0.01 molar solution of sodium dodecyl sulphate (SDS) [9]. During the contacts, both the load and contact radius were measured through a load sensor and an optical microscope. Equation (6) was used to fit the data of the load and contact radius to find the work of adhesion. Also, experiments using gelatine spheres with various radii in dry contact with a Perspex flat were done and the results from the pull-off force were found in close agreement with the JKR theory while for a rubber sphere in dry contact with a rubber flat, the results from the pull-off force were found to vary widely due to viscos effects.

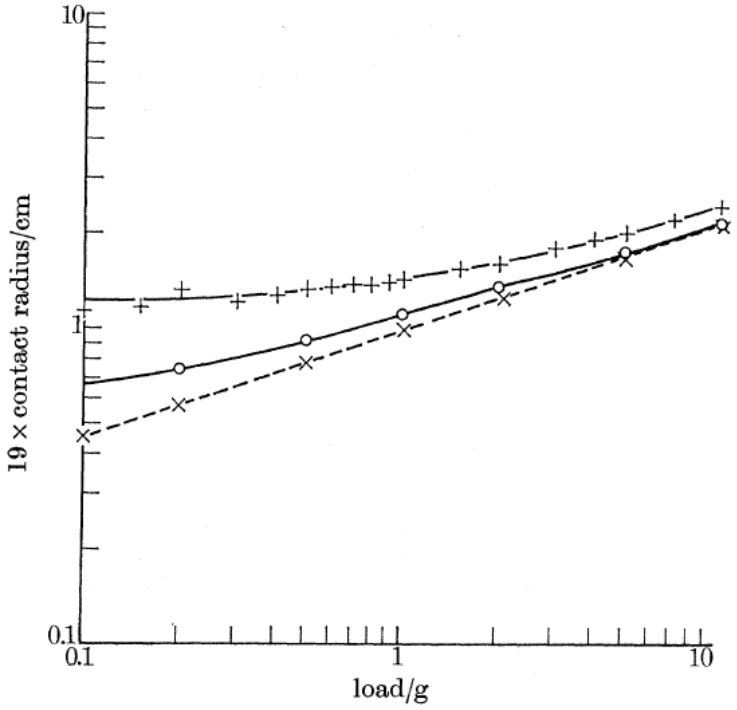

Figure 9: Contact radius vs. the load for two rubber spheres in dry and lubricated contact.

+, dry contact; O, water contact; ×, SDS solution contact; —— , JKR theory; ---- Hertz theory [9].

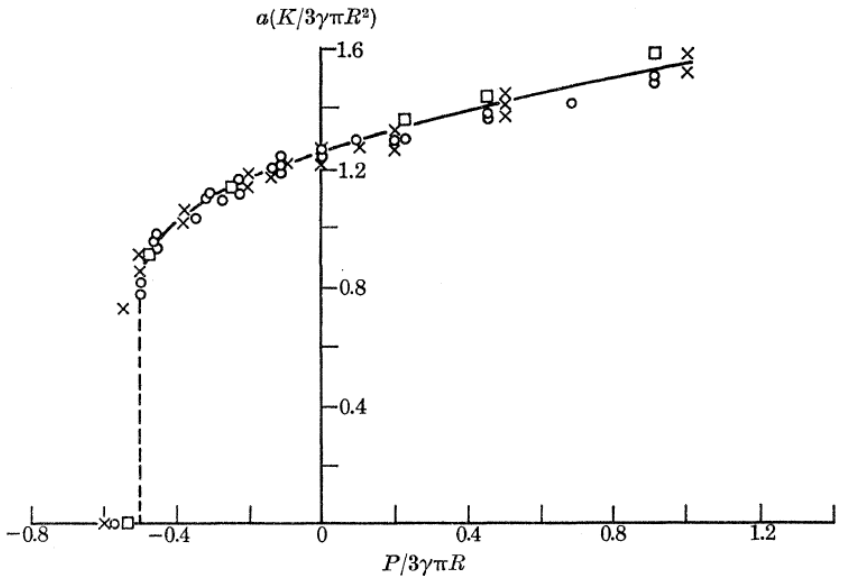

Figure 10: Contact radius vs. the load of gelatin sphere in dry contact with Perspex flat.

O, 2.45 cm radius; ×, 7.9cm radius; □, 25.5cm radius; —— JKR theory [9].

Since then, the JKR theory has been widely used to study adhesion between soft materials. In 1991, Chaudhury and Whitesides studied the work of adhesion of PDMS (Sylgard 170) in the air and liquid media. Both the load and contact radius were measured and the curve of a^3 as a function of P was plotted and fitted with equation (6) to find the work of adhesion W and the elastic parameter K [24]. Also, the pull-off force was used to obtained the work of adhesion for semispherical lenses with radii varying from 1 to 2 mm. Results obtained from the two different methods were very close. For the unmodified PDMS, there was almost no hysteresis while for functionalized PDMS, the hysteresis was not negligible and the work of adhesion obtained from the pull-off force was consistent with that from the unloading curve fitting. In a later study of the self-adhesion of PDMS (Sylgard 170), hysteresis was observed even for the as prepared samples and the work of adhesion from the loading and unloading curve fittings results were 37 ± 3 mJ/m^2 and 56 ± 3 mJ/m^2, respectively [25]. Also, the PDMS samples

extracted with chloroform were tested and the work of adhesion from the loading and unloading curve fittings were 39±2 mJ/m^2 and 328±3 mJ/m^2, respectively.

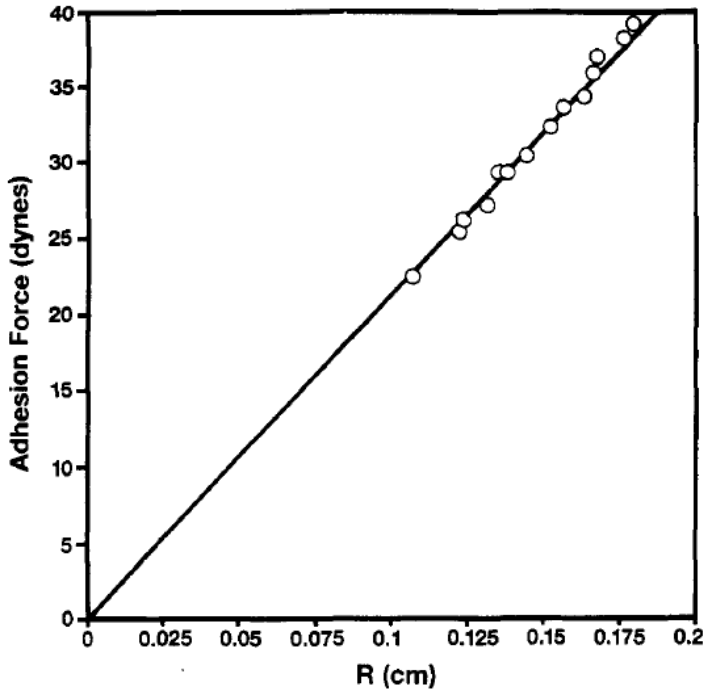

Figure 11: Pull-off force between PDMS lens and sheets varying linearly with the radius of the lens. The work of adhesion obtained from this plot is 45.2 mJ/m^2 [24].

Using the JKR method, Deruelle et al. measured the work of adhesion between a PDMS lens and a silicon wafer covered by a grafted layer of PDMS and it was concluded that interfacial chains play an important role on adhesion [26]. Similarly, the JKR method was also used to measure the work of adhesion between polymer coated PDMS lens and a polymer coated silicon wafer flat [27]. As mentioned in this paper, the authors were not clear whether the JKR theory could be used for such a composite structure.

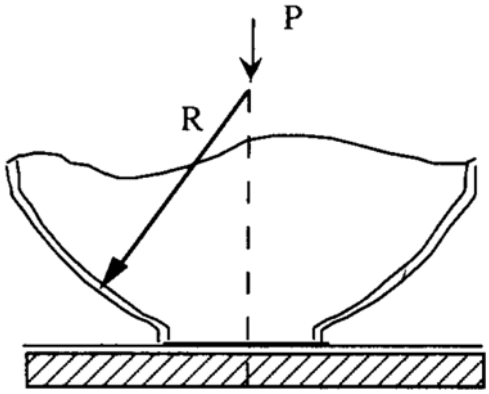

Figure 12: Schematic of a polymer coated PDMS cap in contact with a polymer coated flat surface [27].

In 1997，Choi et al. measured the work of adhesion of vinyl-terminated PDMS with 3 different cross-linker ratios: 1.7, 2.2 and 2.7 with the JKR method [28]. Based on their results of as prepared and extracted PDMS samples, it was concluded that the entanglement of tethered chains and their interdigitation with networks at the interfaces may be the dominant mechanism for the observed hysteresis for extracted samples. However, Perutz et al. studied another model of PDMS with 3 different cross-linker ratios: 1.7, 1.9 and 2.5 and their conclusion was that the hysteresis stems from complexation between the excess cross-linker and the catalyst. In the former paper, hysteresis increases with decreasing cross-linker ratios while in the later paper, hysteresis increases with increasing cross-linker ratios. Of course, one should notice that the PDMS systems used in their studies are different. However, this example demonstrates the complexities concerning the adhesion between soft elastomers.

Using a surface force apparatus (SAF), Maeda et al. found that tethered chains on surfaces will increase the hysteresis and frictional forces [29]. With the JKR tests on PDMS, Amouroux et al. also found that the hysteresis increases with the amount of tethered chains [30]. A. Galliano et al. studied adhesion and friction between PDMS

lenses with two different molecular weights and a glass substrate and their results showed that higher molecular weight PDMS exhibits higher adhesion energy [31].

Chapter 2: Experiments

Contact experiments were done for self-contact of pristine and extracted PDMS, and contact between pristine PDMS lenses and Ecoflex substrates. The work of adhesion from both the loading and unloading curves were obtained based on the pull-in and pull-off forces, respectively. Also, the Young's modulus of pristine PDMS was obtained using the two point formula. Uniaxial tensile tests of pristine PDMS were also performed to measure the Young's modulus and the results are compared to those obtained from the contact experiments. For all of the results, at least three samples were tested to calculate the average values and standard errors.

2.1 SAMPLE PREPARATION

PDMS：Syglard184 (Dow Corning Corporation), the common form of PDMS was used in our experiments. It consists of pre-polymer (base) and cross-linker (curing agent). It is recommended to mix them in a 10:1 weight ratio of the base polymer and curing agent. To study the effect of the mixing ratio, PDMS samples are prepared for 5 different mixing ratios, from 10:1 to 50:1. The mixture is stirred for 10 minutes with a clean glass rod and then degased in a desiccator for one hour to remove the bubbles.

To make PDMS substrates, the degased mixture was poured into a glass petri dish. For the lenses, small droplets of the mixture were placed with a pipette on trichlorosilane treated glass slides. The trichlorosilane treatment to the glass slides makes the removal of the lenses easier after the curing, and it is also helpful to make the droplet form the spherical shape via a specific contact angle. In experiments, the volume of the droplet is set to be 2 μL to form a spherical lens with the radius of curvature varying from 1.3-2.1 mm. Both the PDMS lenses and substrates are fully cured in an oven at 120 °C for 24 hours.

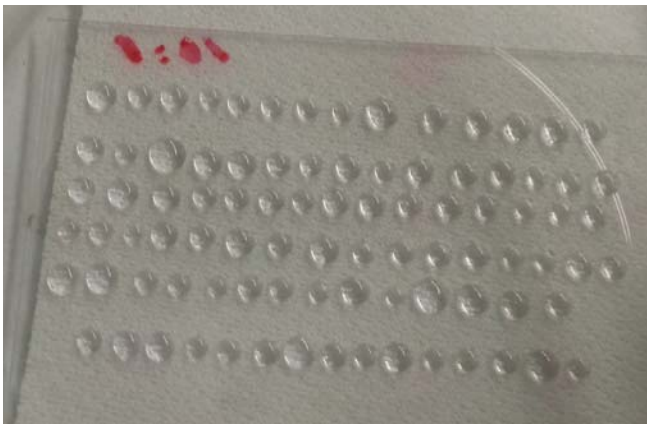

Figure 13: Cured PDMS 10:1 lenses

To remove the uncross-linked monomers on the surface of the PDMS samples, both the lenses and substrates were immersed in chloroform for 24 hours after they are taken out of the oven and cooled into room temperature. Chloroform is a good solvent to swell PDMS and dissolve the uncross-linked oligomers and therefore it is often used to wash PDMS samples [25, 32]. During the soaking, the solvent was changed 3 times. After that, the samples were taken out of the solvent and dried in a desiccator for 24 hours at room temperature.

Ecoflex 0300 is a silicon elastomer containing two parts: Part A and Part B pre-polymers mixed in a 1:1 weight ratio. To prepare Ecoflex 0300 samples, Part B pre-polymer was added first and stirred for 3 minutes with a glass rod and then Part A pre-polymer with the same weight was added and was further stirred for 3 minutes. The mixture was degased for 10 minutes in a desiccator to remove the bubbles induced during the stirring. The mixtures are cured at 70 °C for 4 hours in an oven.

2.2 EXPERIMENTAL APPARATUS

Both the contact and tensile experiments were conducted with a dynamical mechanical analyzer (DMA), RSA G2 to measure the load and displacement. The resolution for the load and displacements are 10 μN and 1 nm, respectively. To measure the radius of curvature of the PDMS lenses, a Zeiss microscope was used to observe the side view and the images of the PDMS lenses were read into a Matlab code to calculate their radii of curvature. The load penetration data was exported directly from the TRIOS software for RSA G2.

Figure 14: Experimental Apparatus: Zeiss microscope and RSA G2, DMA.

2.3 CONTACT EXPERIMENTS

The main procedures for the contact experiments are shown in the figure below. After sample preparation, the lenses were observed under the microscope. The samples

displaying dusts or other contaminations on the surfaces were not used in the contact experiments.

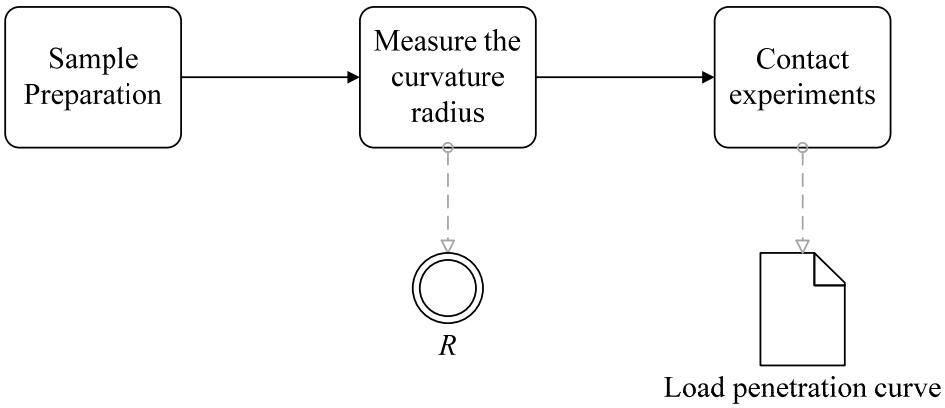

Figure 15: Experimental procedure for contact experiments.

To measure the radius of curvature, the PDMS lenses were placed on a glass slide and their side views were observed under a microscope. Clear pictures with high magnification (30X or 35X) were taken and the pixel information was recorded and imported to a Matlab code to calculate the radius of curvature.

Figure 16: PDMS lens on a glass slide observed under a microscope from the side view.

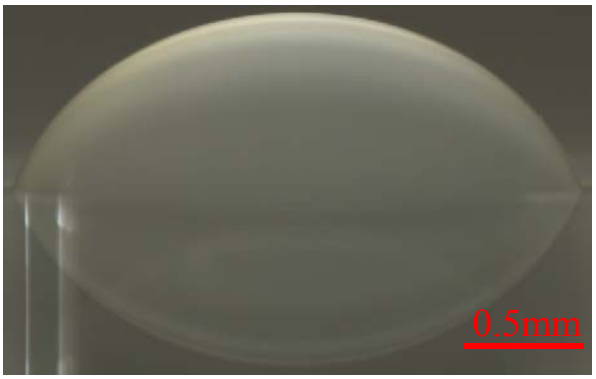

Figure 17: Side view of a PDMS lens.

To calculate the radius of curvature, a Matlab code was written to read the pictures and track the edge. The coordinates of the edge were fit to a circle to find the radius and then the radius of the lens was outputted based on the corresponding pixel information. To be consistent, only the central part of each lens that contacted with the substrates were fitted. From the figure below, we can see that the fitted circle is very close to the profile of the PDMS lens, especially for the middle part.

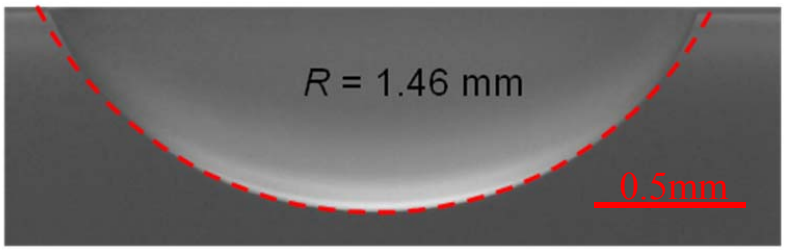

Figure 18: PDMS lens and the fitted circle (red dash line).

For the contact experiments, the PDMS lens was attached to the top compressive geometry and the corresponding substrate was placed on the bottom counterpart. The PDMS lenses adhered to the metal plate very well so it is not necessary to use any glue or scotch tape to affix them. However for the substrate, sometimes a double sided scotch

tape was used to strengthen the adhesion between the substrate and the bottom metal plate.

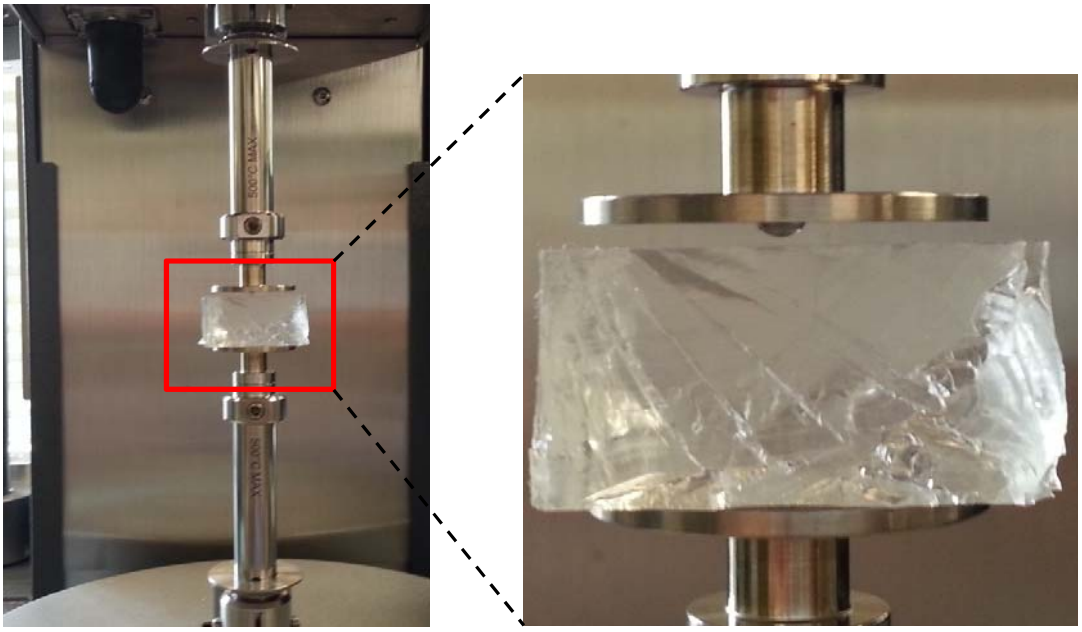

Figure 19: Experimental setup.

A Hencky strain rate of 2×10^{-4} /s was used in the TRIOS settings to control the actual loading and unloading rates. For all of the contact experiments, the actual loading and unloading rates are about 100 nm/s.

Before running the experiments, the two samples were brought as close together as possible without any contact by manual operations of the RSA G2 and visual observation. Then the experiment was initiated at a rate of about 100 nm/s. It takes a while before the two samples start to contact. When the contact occurs, the force will jump to negative (tensile) due to interactive attractions between the two samples. As the penetration increases, the force will turn into compressive. When the compressive force

reached the desired preload (about 1-2 mN), the unloading step was initiated and it lasted until the two samples separated.

2.4 TENSILE EXPERIMENTS

Uniaxial tensile tests were conducted for pristine PDMS and Ecoflex samples. The cured samples were cut into rectangular strips with an original length of about 70 mm and width of around 10 mm. The thickness of the samples varies from 1 to 2 mm, which is close to the radius of curvature of the lens tested in contact experiments. The sample was mounted between the two tensile geometries with a paper frame. After mounting the samples, the sides of the frame were cut. The gauge length between the tensile geometries is about 65 mm, therefore the ratio of the gauge length to the width is larger than 5 for all samples to reduce any boundary effects.

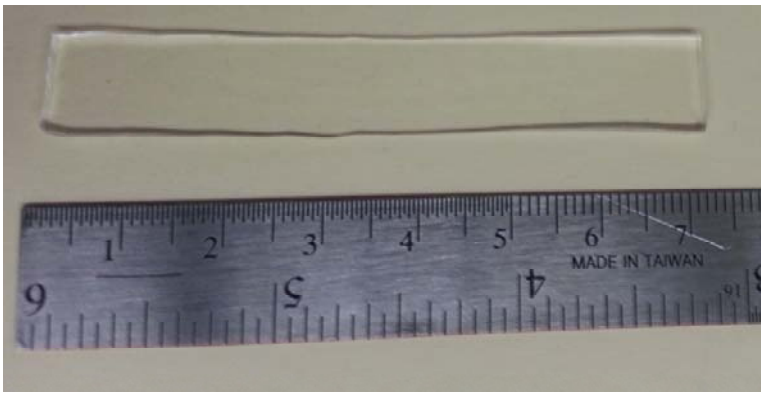

Figure 20: One PDMS strip.

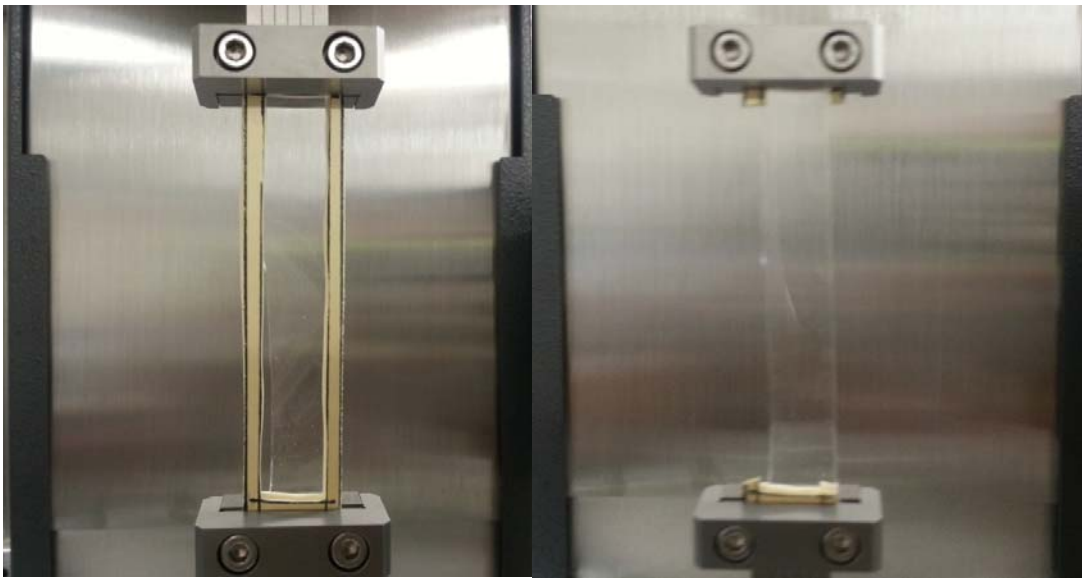

Figure 21: a) PDMS sample was mounted with a paper frame. b) The sides of the paper frame are cut away after the mounting.

About 10% strain was applied to all samples with a loading and unloading process. For PDMS samples, both the loading and unloading rates are 0.04mm/s while for Ecoflex samples, a slower rate 0.0223mm/s was used to reduce the viscoelastic effect.

Chapter 3: Results and Discussions

3.1 The self-adhesion of PDMS with different mixing ratios

From the software of the DMA, the load and displacement were exported and analyzed. To reduce the effect of the noise in the data, an average was taken for each ten points. The figure below shows one example of the load penetration curve of pristine PDMS 10:1.

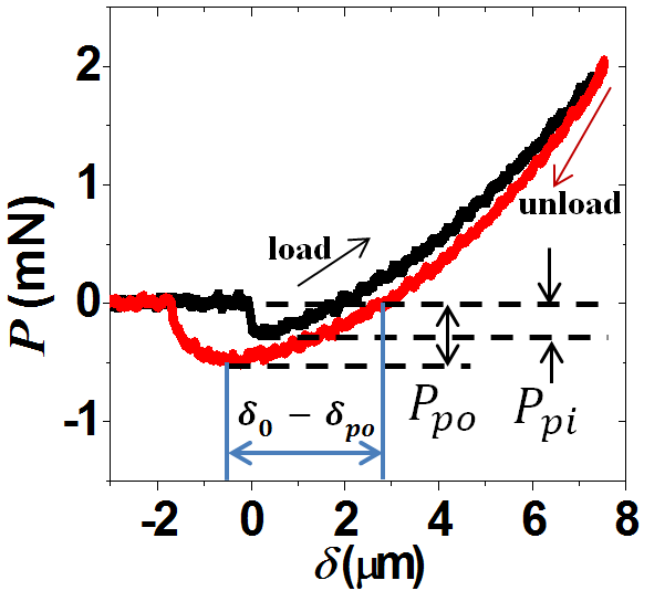

Figure 22: Load penetration curve for pristine PDMS 10:1.

From the figure above, we see that initially, the force was zero and then as the samples get close to each other, the force jumps to negative at the pull-in. Then, the compressive force increases with the penetration. Without dwelling, the unloading started when the force approached the setting preload (around 1-2 mN). When the force decreased to a negative maximum value, the two samples separated with each other and the force returned to zero. A small hysteresis was observed as shown in the figure. The pull-in and pull-off forces were measured.

Using the pull-in and pull-off equations (8) and (9), the work of adhesion W during the loading and unloading are obtained for pristine PDMS samples with 5 different mixing ratios. The results are plotted in the figure below.

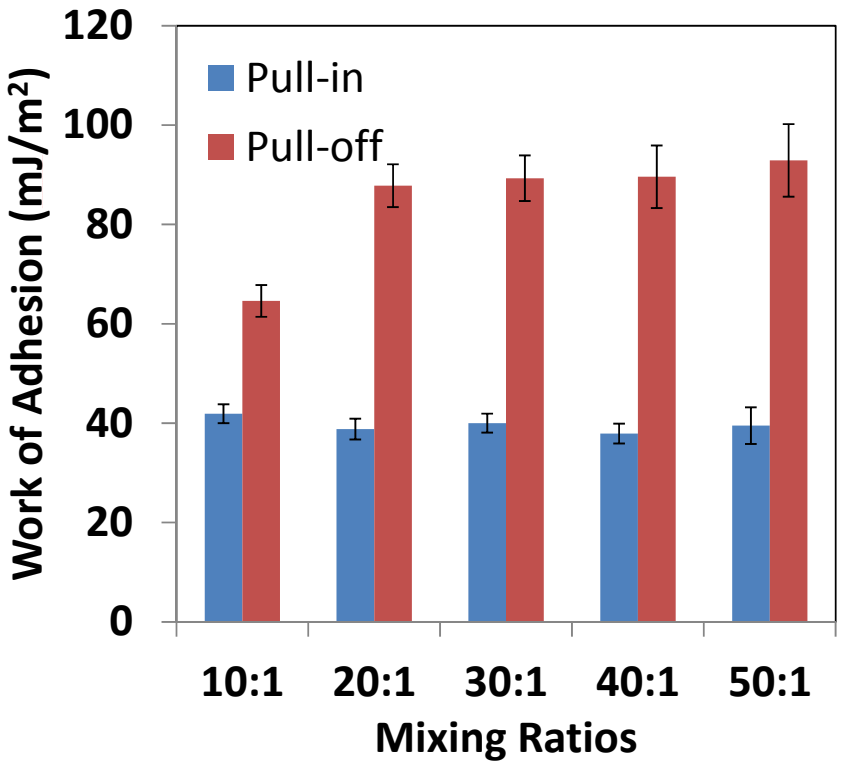

Figure 23: Self-adhesion of pristine PDMS with different mixing ratios.

The work of adhesion obtained from the pull-in and pull-off forces for PDMS 10:1 are 41.9±1.9 mJ/m^2 and 64.6±3.2 mJ/m^2 respectively, which agree quite well with the values in the literature [18, 33, 34]. As the mixing ratios increases, there is no obvious difference in the pull-in work of adhesion. However, for the pull-off work of adhesion, it increases to 87.8 mJ/m^2 for PDMS 20:1 and then doesn't change much for the larger mixing ratios.

3.2 THE SELF-ADHESION BETWEEN EXTRACTED PDMS SAMPLES

The same contact experiments were done on PDMS samples extracted with chloroform for the same five different mixing ratios. The results are plotted in the figure below.

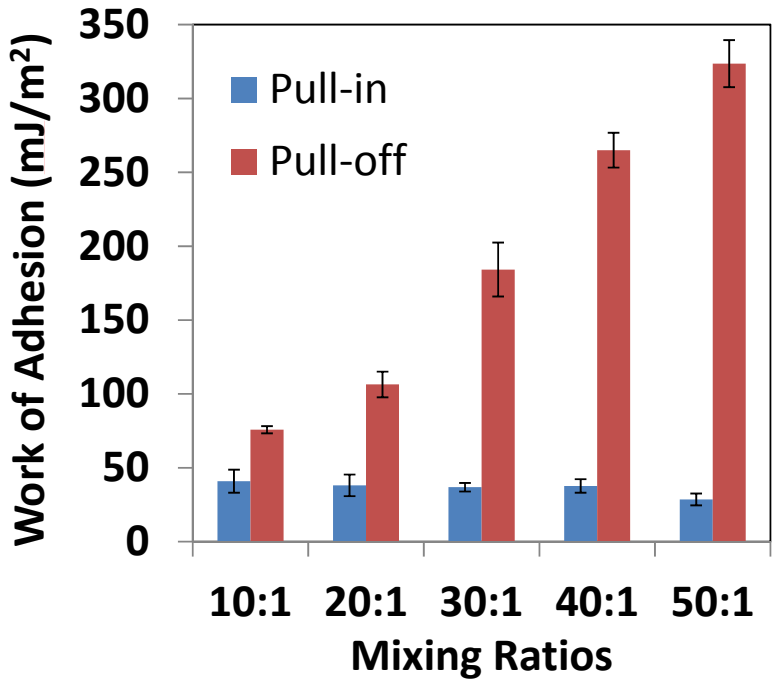

Figure 24: Self-adhesion of extracted PDMS with different mixing ratios.

For the pull-in work of adhesion, the results are similar except that the result for PDMS 50:1 is smaller than the other four PDMS samples. Considering the relatively high noise in the force measurement, the relative error in the pull-in force measurement could be as much as 20%. Therefore, to differentiate the pull-in force between different mixing ratios, a higher resolution of the force measurement and a less noisy environment are required.

For the pull-off work of adhesion, all the extracted PDMS samples showed a higher value than the corresponding pristine PDMS samples with the same mixing ratios. Also, there is an obvious difference between the two trends: for pristine PDMS samples, the value reaches a plateau from the 20:1 mixing ratio while for extracted PDMS samples, the value keeps increasing until the 50:1 mixing ratio and up to 323.6 mJ/m^2.

3.3 The adhesion between PDMS and Ecoflex

Apart from the self-adhesion of pristine PDMS and extracted PDMS, the foreign contact between pristine PDMS and Ecoflex was also tested. The results were plotted in the figure below.

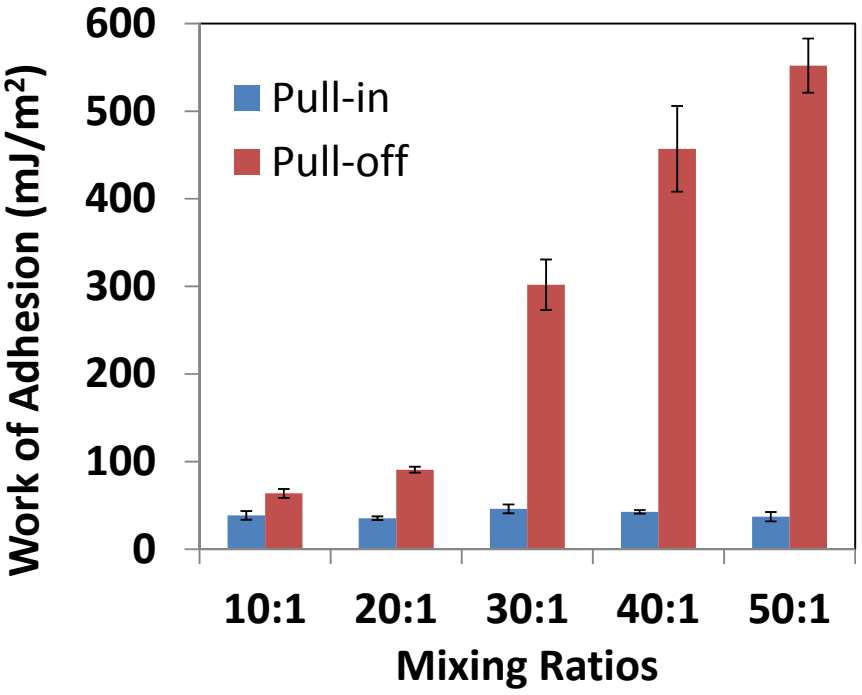

Figure 25: Foreign-adhesion of pristine PDMS with different mixing ratios and Ecoflex.

From the figure, we can see that the pull-in work of adhesion again remains pretty much the same for different mixing ratios while the pull-off work of adhesion increases with the increasing mixing ratios and reaches 552 mJ/m^2 for pristine PDMS and Ecoflex.

3.4 THE YOUNG'S MODULUS OF THE PDMS SAMPLES

From the load penetration curve, the penetration corresponding to the zero load and pull-off can be measured. Using the two-point equation (10), the combined modulus could be calculated. Assuming the Poisson's ratio to be 0.5, Young's moduli of pristine PDMS were derived.

For the tensile tests, the stress-strain curves were plotted for different pristine PDMS. From the figure below, we can see that the stress is quite linear with strain although small hysteresis was also observed. Young's moduli were also obtained by linear fitting of the loading curve. Results from the two different experiments are summarized in the table.

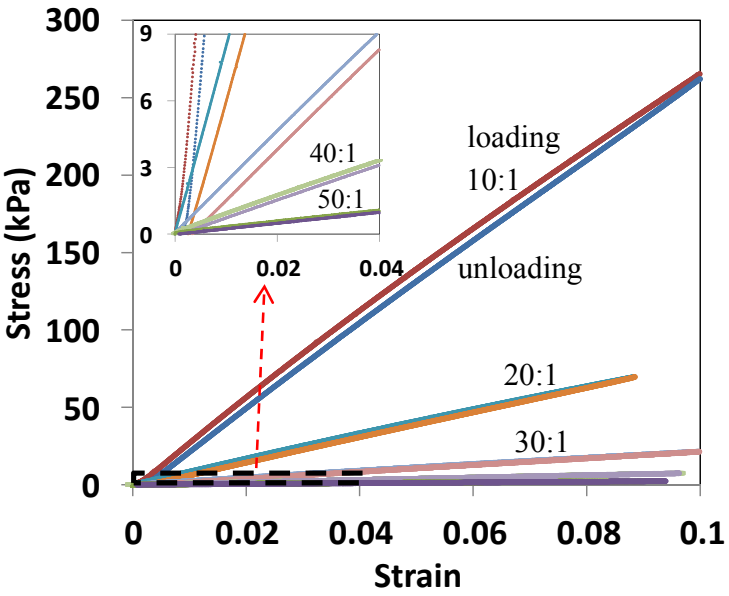

Figure 26: Stress-strain curves of pristine PDMS. For each type of PDMS, both loading and unloading curves were plotted. The loading curve is at the top and the unloading curve is at the bottom as indicated for PDMS 10:1.

Pristine	10:1	20:1	30:1	40:1	50:1
JKR (MPa)	2.73±0.30	0.896±0.113	0.249±0.012	0.1±0.009	0.029±0.002
Tensile (MPa)	2.99±0.20	0.841±0.030	0.232±0.008	0.072±0.001	0.0237±0.0007

Table 1: Young's modulus of pristine PDMS.

For PDMS 10:1 to 30:1, results from the JKR method agree with that from tensile tests within the experimental error. For PDMS 40:1 and 50:1, there are some discrepancies between the two results. One difference between the two experiments is that the loading rates for the JKR and tensile tests are 100 nm/s and 0.0233 mm/s, respectively. However, according to the viscoelastic theory, with a slower loading rate,

results from the JKR experiments should exhibit a lower Young's modulus which is contrary to our experimental results. One possible reason could be that at zero loads, the contact radius is not small enough compared to the radius of curvature of the lens. Therefore δ_0 is actually smaller than that predicted by the JKR theory using the parabolic approximation. For pristine PDMS 40:1 and 50:1, the values of m are found to be around 6.97 and 4.77. A more detailed analysis of the effect of m on the combined modulus E^* calculated with equation (10) would be helpful to answer this question.

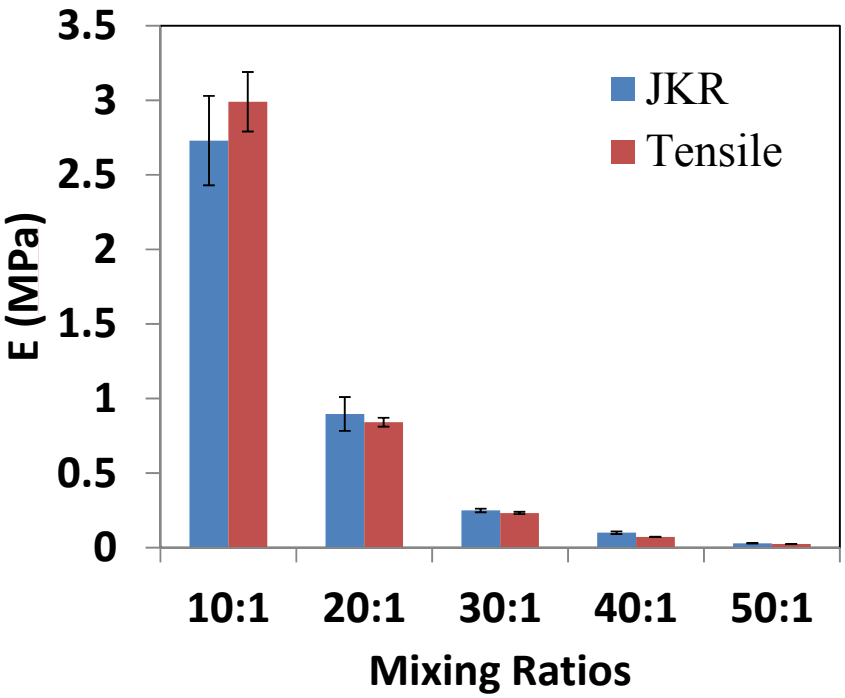

Figure 27: Young's moduli vs. mixing ratios for pristine PDMS.

Also, the tensile tests for Ecoflex were also done and the Young's modulus was found to be 59.0±1.6 kPa, which agrees quite well with the values in the literature [35].

3.5 VALIDATION OF THE EXPERIMENTAL RESULTS

Results from contact experiments are summarized in the table below.

		Self-contact of pristine PDMS	Self-contact of extracted PDMS	Foreign contact between pristine PDMS and Ecoflex
Work of adhesion from pull-in force (mJ/m^2)	10:1	41.9±1.9	40.9±7.8	38.6±4.9
	20:1	38.8±2.1	38.1±7.3	35.4±2.0
	30:1	40.0±1.9	36.9±2.9	34.8±4.4
	40:1	37.9±2.0	37.7±4.6	42.7±2.0
	50:1	39.5±3.7	28.6±4.0	37.0±3.2
Work of adhesion from pull-off force (mJ/m^2)	10:1	64.6±3.2	75.8±2.4	63.7±5.1
	20:1	87.8±4.3	106.4±8.7	90.8±3.4
	30:1	89.3±4.6	184.2±18.2	302.0±28.9
	40:1	89.6±6.3	265.0±11.8	430.1±24.0
	50:1	92.9±7.3	323.6±15.9	552.1±24.4

Table 2: Summary of contact experimental results on the work of adhesion.

To check the inequality (11), the minimum Tabor parameter in our experiments was calculated with smallest work of adhesion $W = 28\,\mathrm{mJ/m^2}$, the largest Young's modulus, $E = 3\,\mathrm{MPa}$, the lower limit of the radius of curvature $R = 1\,\mathrm{mm}$ and the equilibrium spacing $z_0 = 0.3nm$ and the result is $\mu_{\min} = 1936$, which is much larger than 5. Therefore, the first requirement is satisfied for all experiments. Generally, for most soft elastomers, this requirement is easy to satisfy.

For the validation of the inequality (12), the maximum adhesion parameter α was calculated with highest possible work of adhesion $W = 1000\,\mathrm{J/m^2}$, the higher limit of the radius of curvature $R = 2$ mm, the lowest Young's modulus, $E = 23.7\,\mathrm{kPa}$ and the lower limit of the thickness $h = 10\,\mathrm{mm}$. The results is $\alpha_{\max} = 0.016$, which is smaller than 0.02. Therefore the second requirement is satisfied for all experiments.

To check the inequality (13), we must interrogate it case by case since it is not satisfied for all of the experiments. Young's moduli from tensile tests are used in the calculations and the Poisson's ratio is assumed to be 0.5 for both PDMS and Ecoflex.

For the pull-in work of adhesion, the minimum value of m was calculated with the lowest Young's modulus for PDMS 50:1, the approximate work of adhesion 44 $\mathrm{mJ/m^2}$ and the approximate radius of curvature 1.5 mm. The result is $m = 6.31$, which means the third requirement is satisfied for all pull-in work of adhesion measurements.

Next, the pull-off work of adhesion was considered.

For pristine PDMS 40:1, the work of adhesion is 89.6 $\mathrm{mJ/m^2}$ and the Young's modulus obtained from tensile tests is 72 kPa. With an approximate radius of curvature of 1.5mm, the value of m is found to be 6.97. For pristine PDMS 10:1 to 30:1, they have a lower pull-off work of adhesion and higher Young's modulus and the corresponding value of m is going to be even larger. Therefore, for pristine PDMS 10:1 to 40:1, their values of m are larger than 5. For pristine PDMS 50:1, $m = 4.77$ which is a bit smaller than 5.

Using the same method, the value of m for extracted PDMS 30:1 and 40:1 are 8.12 and 4.88. Therefore, the requirement of inequality (13) is satisfied for extracted PDMS 10:1 to 30:1.

For the contact between pristine PDMS 30:1 and 40:1 with respect to Ecoflex, m is equal to 5.09 and 4.00. Therefore, the requirement of inequality (13) is satisfied for the contact between pristine PDMS 10:1 to 30:1 and Ecoflex.

	Self-contact of pristine PDMS	Self-contact of extracted PDMS	Foreign contact between pristine PDMS and Ecoflex
10:1	26.98	25.58	9.22
20:1	15.96	14.97	8.06
30:1	10.33	8.12	5.09
40:1	6.97	4.88	4.00
50:1	4.77	3.14	2.97

Table 3: The dimensionless parameter m for all experiments. The green colored values do not satisfy the inequality (13).

For the tests with m smaller than 5, an iterative Matlab code is written to correct the work of adhesion. The iteration will terminate when the difference of m between the last iteration and the new iteration is smaller than 0.001 or the maximum iteration is reached.

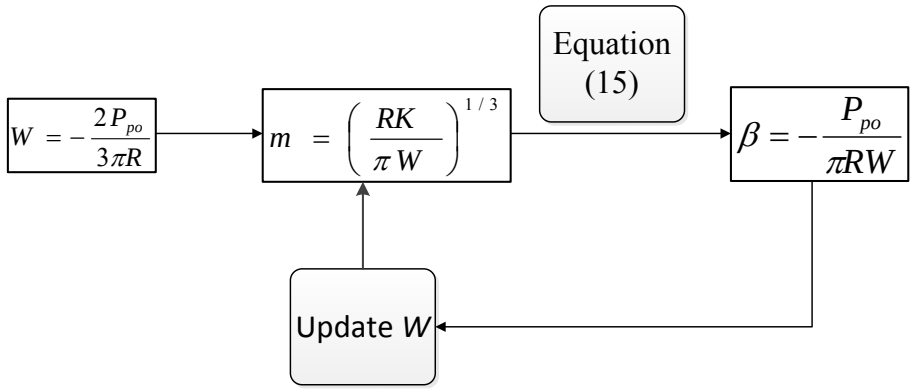

Figure 28: Flow chart of the iterative code.

After the correction, the updated results are summarized in the table below.

		Self-contact of pristine PDMS	Self-contact of extracted PDMS	Foreign contact between pristine PDMS and Ecoflex
Work of adhesion from pull-in force (mJ/m^2)	10:1	41.9±1.9	40.9±7.8	38.6±4.9
	20:1	38.8±2.1	38.1±7.3	35.4±2.0
	30:1	40.0±1.9	36.9±2.9	34.8±4.4
	40:1	37.9±2.0	37.7±4.6	42.7±2.0
	50:1	39.5±3.7	28.6±4.0	37.0±3.2
Work of adhesion from pull-off force (mJ/m^2)	10:1	64.6±3.2	75.8±2.4	63.7±5.1
	20:1	87.8±4.3	106.4±8.7	90.8±3.4
	30:1	89.3±4.6	184.2±18.2	302.0±28.9
	40:1	89.6±6.3	270.0±12.3 (265.0±11.8)	442.4±24.9 (430.1±24.0)
	50:1	95.4±7.7 (92.9±7.3)	337.3±17.5 (323.6±15.9)	583.8±26.9 (552.1±24.4)

Table 4: Summary of the work of adhesion after correction. Green colored values are the updated values after correction and the values in the parentheses are the work of adhesion before correction.

The updated results after the correction are plotted in the following figures.

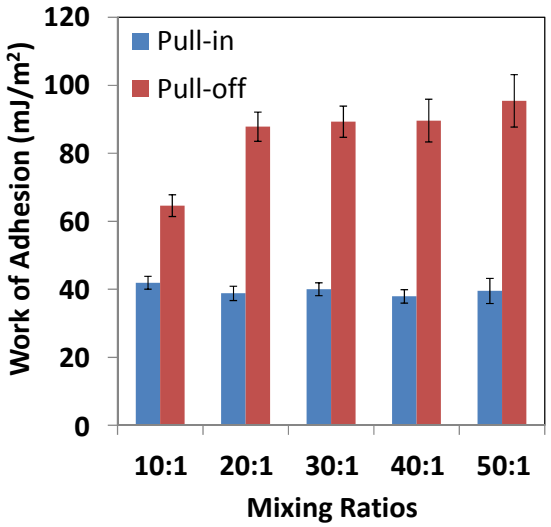

Figure 29: The updated work of adhesion for pristine PDMS

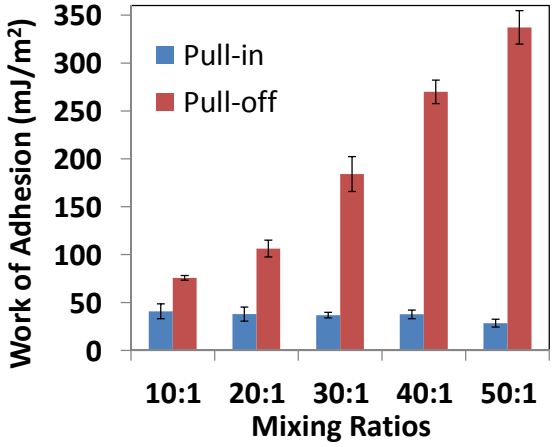

Figure 30: The updated work of adhesion for extracted PDMS

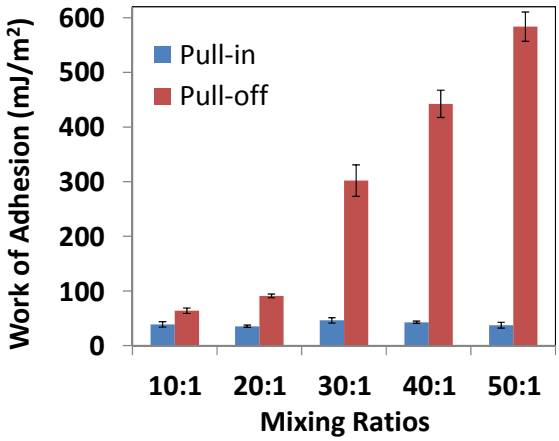

Figure 31: The updated work of adhesion between pristine PDMS and Ecoflex.

3.6 DISCUSSIONS

Due to hysteresis, the pull-off work of adhesion are higher than the pull-in work of adhesion for all experiments.

For pristine PDMS samples, the pull-off work of adhesion increases greatly from 10:1 to 20:1. Since 10:1 is the recommended mixing ratio for PDMS, it is expected that most of the chains are cross-linked such that on the surface, there are only a few of tethered chains (with only one end cross-linked) and free chains (with both two ends free). As the mixing ratios increases, more polymer chains are added and therefore the material will contain more free and tethered chains on the surface. Since tethered chains will enhance the work of adhesion by entanglement and penetration during the unloading process [29, 30], PDMS with a higher mixing ratio is expected to have stronger adhesion. However, the pull-off work of adhesion does not increase too much for further increasing of the mixing ratios. Therefore, it is concluded that there might be another mechanism that will reduce the pull-off work of adhesion for PDMS samples with higher mixing ratios.

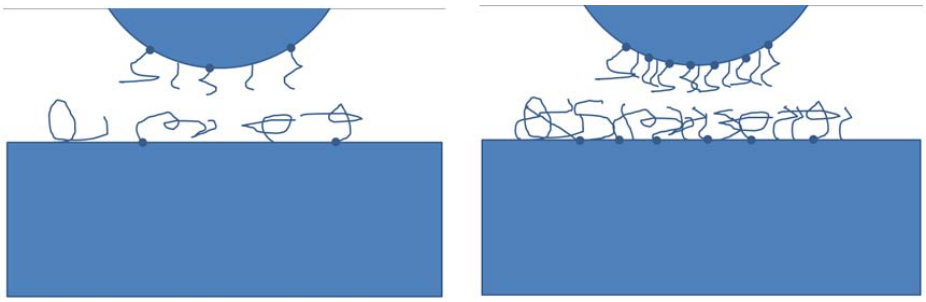

Figure 32: Schematic view of surfaces of pristine PDMS 10:1 (left) and 30:1(right). PDMS with higher mixing ratio contains more free and tethered chains.

Comparing the results from pristine and extracted PDMS samples, it is found that the pull-off work of adhesion is higher for the extracted PDMS samples. After the extraction with chloroform, free chains were removed and only the tethered chains were left on the surfaces. Therefore it is concluded that removing free chains will enhance the pull-off work of adhesion. So the question is how do free chains reduce the adhesion for pristine PDMS samples? Since free chains cannot transmit stress with both ends free, they will be transferred from one surface to the other easily during the contact without a significant contribution to the adhesion in comparison to that of the tethered chains. The existence of these free chains will reduce the chances of the tethered chains entangling with each other and penetrating into the networks. Therefore, for pristine PDMS samples with higher mixing ratios, although they have more tethered chains on the surfaces, the existence of more free chains almost compensates for the effect of this enhancement. For extracted PDMS samples, with free chains removed from the surfaces, the pull-off work of adhesion is expected to increase with the amount of the remaining tethered chains. That is why the pull-off work of adhesion of pristine PDMS does not increase much from 20:1 while that of the extracted PDMS samples continues to increase from 10:1 to 50:1.

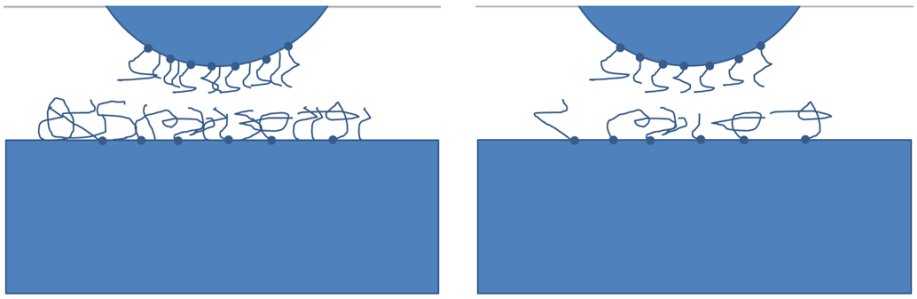

Figure 33: Schematic view of surfaces of pristine (left) and extracted (right) PDMS 30:1. Extraction removes free chains.

For Ecoflex substrates, the free and tethered chains on the surface are similar to pristine PDMS 10:1. Therefore, for foreign contacts between pristine PDMS samples and Ecoflex, the entanglement of PDMS and Ecoflex chains should also be scarce. For higher mixing ratios, PDMS samples contains both more free and tethered chains and they both can penetrate into the Ecoflex networks. It is deduced that the penetration of tethered chains of PDMS into the Ecoflex network increases the work of adhesion during the pull-off force. The existence of more free chains for pristine PDMS samples with a higher mixing ratio seems to not be enough to compensate for the effect of the tethered chains.

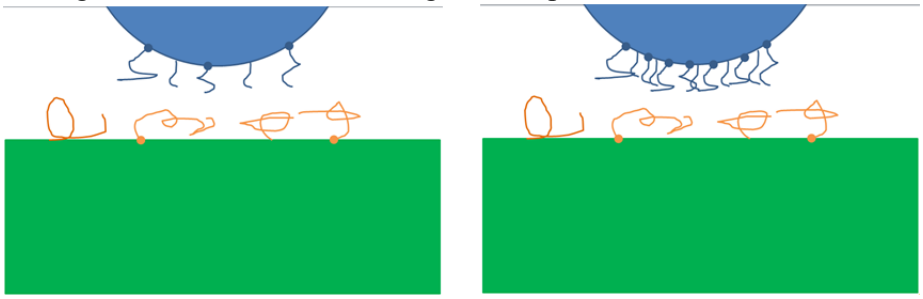

Figure 34: Schematic view of surfaces of pristine PDMS lens for 10:1 (left), 30:1 (right) and Ecoflex (substrates).

It may be surprising to see that there is no obvious difference in the pull-in work of adhesion for the five different mixing ratios. Recall that at the pull-in, the two samples have barely contacted and all the chains have not entangled or penetrated into the

networks. Therefore, the pull-in work of adhesion is independent of the amount of free and tethered chains. For the same reason, the results from pristine and extracted PDMS are also close.

In our experiments, only the third requirement, $m > 5$ is not satisfied for five contact pairs while the first requirement, $\mu > 5$ is relatively easy to satisfy for all tested material combinations. Combining the inequalities of (11) and (13), we could obtain the following inequality

$$R > \max\left(\frac{125 z_0^3 E^{*2}}{W^2}, \frac{375\pi W}{4E^*}\right). \tag{16}$$

Once the radius of curvature is decided, the inequality (12) can be imposed to determine the thickness of the substrate and the result is given here.

$$h > 10\left(\frac{5R^2 W}{\bar{E}_1}\right)^{1/3} \tag{17}$$

Thus, to fully satisfy the three requirements, one could follow a standard procedure given in the figure below to design the dimensions of the samples in experiments.

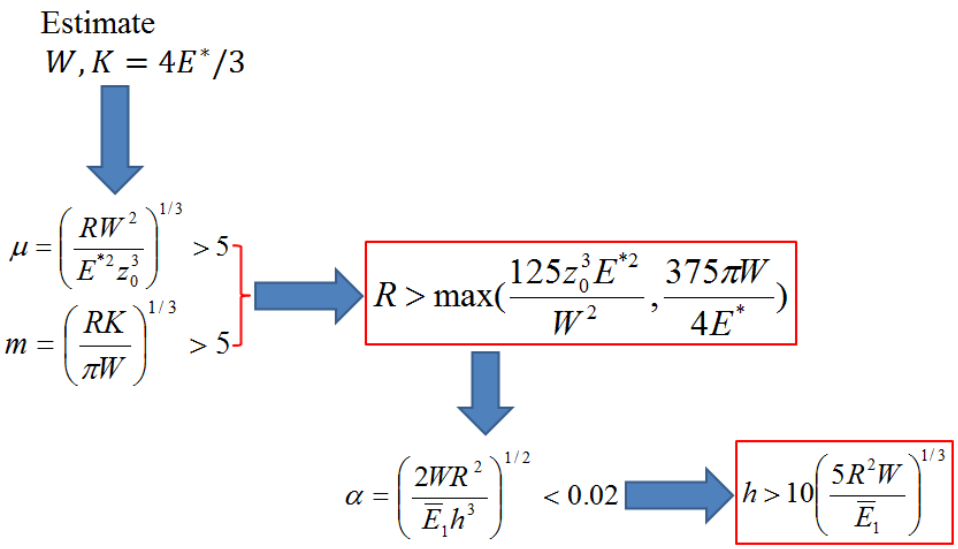

Figure 35: Procedure to design the sample dimensions.

Chapter 4: Conclusions and Future Work

4.1 SUMMARY AND CONCLUSIONS

In this report, first, the JKR theory was summarized and the following three important parameters were proposed to validate the experimental results.

(1) The Tabor parameter: $\mu > 5$

(2) The adhesion parameter: $\alpha < 0.02$

(3) The third dimensionless parameter: $m > 5$

To fully satisfy the three requirements, a practical procedure to design the sample dimensions was proposed.

Based on the JKR theory, the pull-in force formula was derived and proposed to calculate the work of adhesion from the loading curve approximately. There are several advantages of this formula. First, it is simple and straightforward as the pull-off force formula. The pull-off force is often used to obtain the work of adhesion from the unloading curve and the pull-in force can be used to obtain the work of adhesion from the loading curve. Second, it is independent of some factors such as preload and contact time since the pull-in occurred at the very beginning of the contact. Last but not least, it will save a significant amount of experimental time especially when experiments are run at a very slow rate compared to the pull-off force formula since the pull-off occurs near the end of separation. However, it also has some limitations. First, it is smaller than the pull-off force and therefore requires a higher resolution of the force measurement and a less noisy environment to obtain the same accuracy. Second, it can only be used as an approximate method to calculate the work of adhesion since it is difficult to determine the exact contact point given a load penetration curve.

Guided by the given requirements, contact experiments were designed to measure the work of adhesion of PDMS with 5 different mixing ratios using a substrate with

thickness larger than 10 mm. With DMA, contact experiments were done on the self-contact of pristine PDMS and extracted PDMS for 5 different mixing ratios from 10:1 to 50:1. The foreign contact between the 5 different pristine PDMS and Ecoflex were also studied. Our results for pristine PDMS 10:1 agree well with the values in the literature.

Experimental results showed that the pull-in work of adhesion is generally the same for pristine and extracted PDMS samples with 5 different mixing ratios. Also, there is no significant difference between the pull-in work of adhesion between pristine PDMS and Ecoflex. The pull-off work of adhesion for pristine PDMS samples increases greatly when the mixing ratio is increased from 10:1 to 20:1 but does not increase too much for further higher mixing ratios. For extracted PDMS samples, the pull-off work of adhesion increases significantly when the mixing ratio varies from 10:1 to 50:1. A similar trend is also observed for the contact of pristine PDMS and Ecoflex.

To explain the complex adhesion behaviors, the roles of both the free and tethered chains are taken into account with the assumption that higher mixing ratio results in more free and tethered chains. While the entanglement and penetration of tethered chains can enhance the work of adhesion significantly, that of free chains cannot. Therefore, with higher mixing ratios, the existence of more free chains could reduce the chances of tethered chains entangling with each other and penetrating into the network during the contact, which therefore could potentially compensate for the enhancement by tethered chains.

4.2 FUTURE WORK

From the JKR theory and our trial experimental results, we see that the thickness of the substrate plays an important role on the pull-off force. However, quantitative comparisons between the experiments and theory is still lacking. Therefore, one direct

way to study this effect is to prepare PDMS substrates with different thicknesses and measure their pull-off force from the PDMS lens with the same radius of curvature. Once the effect of the substrate thickness is known, we can use this property to tune the pull-off force by changing the thickness of the substrates.

To enhance the work of adhesion of PDMS, another technique is to do the UVO treatment. Experimental results in the literature show that UVO treatment can enhance the pull-off work of adhesion [36].

As we also know, there are many other factors that could significantly affect the work of adhesion such as humidity, temperature, surface roughness, loading rate and so on. Since our DMA machine, RSA G2 is equipped with a forced convection oven (FCO), it is convenient to measure the work of adhesion at high temperatures up to 500 °C. To run the tests at low temperatures, a nitrogen cooling system could be installed to reach a temperature as low as -150 °C. Also, with the TRIOS software, it is feasible to test the work of adhesion at different loading and unloading rates.

Since it is difficult to control the humidity for RSA G2, a JKR apparatus with a humidity chamber was also built to study the effect of humidity on the work of adhesion. With this apparatus, humidity inside the chamber can be controlled and both the load and contact radius can be measured at the same time. The work of adhesion could be obtained by the pull-in and pull-off forces directly or by doing the curve fittings with equation (6).

Adhesion between other materials can be measured with the JKR method such as adhesion between PDMS and grapheme or Mos2, adhesion between gold and soft biological tissues.

Appendix A: Matlab codes to calculate the curvature radius of PDMS lens

```
% This program is for tracking the edges of PDMS lems and outputing the
% curvature radius.
% First the image is read into memory; then it is thresholded to show
% edges. A search algorithm is used to get the coordinates of the edges.
% These coordinates are fitted with a circle and the radius is displayed.
clear all; close all;
set(0,'DefaultFigureWindowStyle','docked');

%% the first entering: the name and format of the picture
Image_1 = imread('1','jpeg'); % reads image from the work director

figure(1);
imshow(Image_1);axis xy;hold on
impixelinfo
%% the second entering: choose the ranges of x and y based on figure (1).
%(X,Y) coordinates at the point of mouse will show
%at the left bottom corner of figure (1)

I2 = Image_1(178:470,1:1388);
% image is cropped to identify the useful region
% First range is y, second is x
figure(2)
imshow(I2); axis xy; hold on;
```

```
I3 = edge(I2,'sobel');
figure(3);
imshow(I3); axis xy; hold on;
impixelinfo

%% Search for the edges and save their coordinates
imax = size(I3,2);
jmax = size(I3,1);
I_xl = zeros(1,imax);
I_yl = zeros(1,jmax);
for i = 1:imax
        for j = 1:jmax
            if I3(j,i) == 1
                I_xl(i) = i;
                I_yl(i) = j;
                break;
            end
        end
end
I_xl(I_xl==0) = [];
I_yl(I_yl==0) = []; %Delete the coordinates with zero elements
[mn,i]=min(I_yl);

%% the third entering: pixle information from the microscope directly
scaling=2.15; % Enter the scaling information here, micrometer/pixel
```

```
                    % 1.84 for 35X
                    % 2.15 for 30X

%% the forth entering: determined by the estimated contact radius
% the default value is 1000 micrometer
a=1000; % Enter the maximum radius of contact area for fitting (micrometer)
j=I_xl(i)-a/scaling;
k=I_xl(i)+a/scaling;
low=int16(j);
high=int16(k);
[x1,x2,x3]=find(I_xl>low&I_xl<high);
I_x=I_xl(x2);
I_y=I_yl(x2);

%Try to fit the circle
[xc,yc,Re,a] = circfit(I_x,I_y);

%Reconstruct the circle from data
  th = linspace(0,2*pi,100)';
  xe = Re*cos(th)+xc; ye = Re*sin(th)+yc;

  R=scaling*Re/1000;    % Calculte the radius with unit mm

figure(2); plot(I_x,I_y,'g.');
figure(3); plot(I_x,I_y,'g.');
```

```
text(I_xl(i),I_yl(i)+10,sprintf('R=%g mm',R))

figure(4);
imshow(I2); axis xy; hold on;
plot([xe;xe(1)],[ye;ye(1)],'r-','linewidth',2);
title('Fitted Circle')
text(imax/2,jmax/2,sprintf('R=%g mm',R))
hold on

function      [xc, yc, R, a] = circfit(x,y)
%
% [xc yc R] = circfit(x,y)
%
% fits a circle in x, y plane
% x, y are column vector where (x(i), y(i)) is a measured point
% result is the center point (yc, xc) and radius R
% an optional output is the vector of coefficient a describing the circle's equation
%    x^2+y^2+a(1)*x+a(2)*y+a(3)=0
%
% By:    Izhak bucher 25/oct /1991,
% Copyright (c) 1981, Izhak Bucher
% All rights reserved.
% Redistribution and use in source and binary forms, with or without
% modification, are permitted provided that the following conditions are met:
%    * Redistributions of source code must retain the above copyright notice, this
```

```
% list of conditions and the following disclaimer.
%    * Redistributions in binary form must reproduce the above copyright notice,
% this list of conditions and the following disclaimer in the documentation and/or
% other materials provided with the distribution.
% THIS SOFTWARE IS PROVIDED BY THE COPYRIGHT HOLDERS AND
% CONTRIBUTORS "AS IS" AND ANY EXPRESS OR IMPLIED
% WARRANTIES, INCLUDING, BUT NOT LIMITED TO, THE IMPLIED
% WARRANTIES OF MERCHANTABILITY AND FITNESS FOR A
% PARTICULAR PURPOSE ARE DISCLAIMED. IN NO EVENT SHALL
% THE COPYRIGHT OWNER OR CONTRIBUTORS BE LIABLE FOR ANY
% DIRECT, INDIRECT, INCIDENTAL, SPECIAL, EXEMPLARY, OR
% CONSEQUENTIAL DAMAGES (INCLUDING, BUT NOT LIMITED TO
% PROCUREMENT OF SUBSTITUTE GOODS OR SERVICES; LOSS OF
% USE, DATA, OR PROFITS; OR BUSINESS INTERRUPTION) HOWEVER
% CAUSED AND ON ANY THEORY OF LIABILITY, WHETHER IN
% CONTRACT, STRICT LIABILITY, OR TORT (INCLUDING
% NEGLIGENCE OR OTHERWISE) ARISING IN ANY WAY OUT OF THE
% USE OF THIS SOFTWARE, EVEN IF ADVISED OF THE POSSIBILITY
% OF SUCH DAMAGE.
    x=x(:); y=y(:);
    a=[x y ones(size(x))]\[-(x.^2+y.^2)];
    xc = -.5*a(1);
    yc = -.5*a(2);
    R  =  sqrt((a(1)^2+a(2)^2)/4-a(3));
```

Appendix B: Matlab code to correct the work of adhesion for $m < 5$

```
% This code is to study the effect of the dimensionless parameter m and
% do the iteration for correction.
clc;
clear all;

i=1;
m(i)=0;
dm=0.001;
for i=1:10000
A=0:0.001:m(i);
P=3*m(i)/8*(m(i)^2+A.^2).*log((m(i)+A)./(m(i)-A))-3/4*m(i)^2.*A-
sqrt(6)*A.^(3/2);
Pc(i)=min(P);
m(i+1)=m(i)+dm;
i=i+1;
end
% plot(m(1:i-1),Pc,'linewidth',2)

% do the iteration
format long
R=1.871*10^(-3);        % the curvature radius lens
W=422.3*10^(-3);      %    the initial work of adhesion
E1=72*10^3;          %    elastic properties of the lens
```

```
v1=0.5;
E2=60*10^3;          %    elastic properties of the substrate
v2=0.5;
a=3/4*((1 - v1^2)/E1 + (1 - v1^2)/E2);
K=1/a;
M=(R*K/pi/W)^(1/3);
Max=100; %maximum iteration
beta(1)=-1.5;
for j=1:Max
for i=2:10000;
      if abs(M-m(i))<1*10^(-3)
            beta(j+1)=Pc(i);
            n(j)=i;
            break
      end
end
 W=W*beta(j)/beta(j+1);
 M=(R*K/pi/W)^(1/3);
 if j>2
       if n(j)==n(j-1)
             break
       end
 end
end
W
```

Bibliography

1. Arzt, E., S. Gorb, and R. Spolenak, *From micro to nano contacts in biological attachment devices.* Proceedings of the National Academy of Sciences of the United States of America, 2003. **100**(19): p. 10603-10606.
2. Schargott, M., V.L. Popov, and S. Gorb, *Spring model of biological attachment pads.* Journal of Theoretical Biology, 2006. **243**(1): p. 48-53.
3. Kim, D.H., et al., *Silicon electronics on silk as a path to bioresorbable, implantable devices.* Applied Physics Letters, 2009. **95**(13).
4. Viventi, J., et al., *A Conformal, Bio-Interfaced Class of Silicon Electronics for Mapping Cardiac Electrophysiology.* Science Translational Medicine, 2010. **2**(24).
5. Kim, D.H., et al., *Dissolvable films of silk fibroin for ultrathin conformal bio-integrated electronics.* Nature Materials, 2010. **9**(6): p. 511-517.
6. Kim, D.H., et al., *Epidermal Electronics.* Science, 2011. **333**(6044): p. 838-843.
7. Johnson, K.L., *Contact mechanics*. 1985, Cambridge Cambridgeshire ; New York: Cambridge University Press. xi, 452 p.
8. Barthel, E., *Adhesive elastic contacts: JKR and more.* Journal of Physics D: Applied Physics, 2008. **41**(16): p. 163001.
9. Johnson, K.L., K. Kendall, and A.D. Roberts, *Surface Energy and the Contact of Elastic Solids.* Proceedings of the Royal Society of London. A. Mathematical and Physical Sciences, 1971. **324**(1558): p. 301-313.
10. Bradley, R.S., *The cohesive force between solid surfaces and the surface energy of solids.* Philosophical Magazine, 1932. **13**(86): p. 853-862.
11. Derjaguin, B.V., V.M. Muller, and Y.P. Toporov, *Effect of contact deformations on the adhesion of particles.* Journal of Colloid and Interface Science, 1975. **53**(2): p. 314-326.
12. Tabor, D., *Surface Forces and Surface Interactions.* Journal of Colloid and Interface Science, 1977. **58**(1): p. 2-13.
13. Johnson, K.L., *Mechanics of adhesion.* Tribology International, 1998. **31**(8): p. 413-418.
14. Maugis, D., *Adhesion of Spheres - the Jkr-Dmt Transition Using a Dugdale Model.* Journal of Colloid and Interface Science, 1992. **150**(1): p. 243-269.
15. Johnson, K.L. and J.A. Greenwood, *An adhesion map for the contact of elastic spheres.* Journal of Colloid and Interface Science, 1997. **192**(2): p. 326-333.
16. Shull, K.R., *Contact mechanics and the adhesion of soft solids.* Materials Science & Engineering R-Reports, 2002. **36**(1): p. 1-45.
17. Grunlan, J.C., et al., *Preparation and evaluation of tungsten tips relative to diamond for nanoindentation of soft materials.* Review of Scientific Instruments, 2001. **72**(6): p. 2804-2810.
18. Ebenstein, D.M. and K.J. Wahl, *A comparison of JKR-based methods to analyze quasi-static and dynamic indentation force curves.* Journal of Colloid and Interface Science, 2006. **298**(2): p. 652-662.

19. Ebenstein, D.M., *Nano-JKR force curve method overcomes challenges of surface detection and adhesion for nanoindentation of a compliant polymer in air and water.* Journal of Materials Research, 2011. **26**(8): p. 1026-1035.
20. Sun, Y.J., B. Akhremitchev, and G.C. Walker, *Using the adhesive interaction between atomic force microscopy tips and polymer surfaces to measure the elastic modulus of compliant samples.* Langmuir, 2004. **20**(14): p. 5837-5845.
21. Johnson, K.L. and I. Sridhar, *Adhesion between a spherical indenter and an elastic solid with a compliant elastic coating.* Journal of Physics D-Applied Physics, 2001. **34**(5): p. 683-689.
22. Sridhar, I., Z.W. Zheng, and K.L. Johnson, *A detailed analysis of adhesion mechanics between a compliant elastic coating and a spherical probe.* Journal of Physics D: Applied Physics, 2004. **37**(20): p. 2886.
23. Maugis, D., *Extension of the Johnson-Kendall-Roberts Theory of the Elastic Contact of Spheres to Large Contact Radii.* Langmuir, 1995. **11**(2): p. 679-682.
24. Chaudhury, M.K. and G.M. Whitesides, *Direct Measurement of Interfacial Interactions between Semispherical Lenses and Flat Sheets of Poly(Dimethylsiloxane) and Their Chemical Derivatives.* Langmuir, 1991. **7**(5): p. 1013-1025.
25. Silberzan, P., et al., *Study of the Self-Adhesion Hysteresis of a Siloxane Elastomer Using the Jkr Method.* Langmuir, 1994. **10**(7): p. 2466-2470.
26. Deruelle, M., L. Leger, and M. Tirrell, *Adhesion at the Solid-Elastomer Interface - Influence of the Interfacial Chains.* Macromolecules, 1995. **28**(22): p. 7419-7428.
27. Mangipudi, V.S., et al., *Measurement of interfacial adhesion between glassy polymers using the JKR method.* Macromolecular Symposia, 1996. **102**: p. 131-143.
28. Choi, G.Y., S.J. Kim, and A. Ulman, *Adhesion hysteresis studies of extracted poly(dimethylsiloxane) using contact mechanics.* Langmuir, 1997. **13**(23): p. 6333-6338.
29. Maeda, N., et al., *Adhesion and friction mechanisms of polymer-on-polymer surfaces.* Science, 2002. **297**(5580): p. 379-382.
30. Amouroux, N. and L. Leger, *Effect of dangling chains on adhesion hysteresis of silicone elastomers, probed by JKR test.* Langmuir, 2003. **19**(4): p. 1396-1401.
31. Galliano, A., S. Bistac, and J. Schultz, *Adhesion and friction of PDMS networks: molecular weight effects.* Journal of Colloid and Interface Science, 2003. **265**(2): p. 372-379.
32. Lee, J.N., C. Park, and G.M. Whitesides, *Solvent Compatibility of Poly(dimethylsiloxane)-Based Microfluidic Devices.* Analytical Chemistry, 2003. **75**(23): p. 6544-6554.
33. Rundlof, M., et al., *Application of the JKR method to the measurement of adhesion to Langmuir-Blodgett cellulose surfaces.* Journal of Colloid and Interface Science, 2000. **230**(2): p. 441-447.

34. Qi, J., *Measurement of surface and interfacial energies between solid materials using an elastica loop*, 2000, Virginia Polytechnic Institute and State University.
35. Marchal, M., et al., *Towards a framework for assessing deformable models in medical simulation.* Biomedical Simulation, Proceedings, 2008. **5104**: p. 176-184.
36. Olah, A., H. Hillborg, and G.J. Vancso, *Hydrophobic recovery of UV/ozone treated poly(dimethylsiloxane): adhesion studies by contact mechanics and mechanism of surface modification.* Applied Surface Science, 2005. **239**(3-4): p. 410-423.